Exploring a low-cost valorization route for Amazonian cocoa pod husks through thermochemical and catalytic upgrading of pyrolysis vapors

Yanet Villasana[1*], Sabino Armenise[2], Javier Ábrego[3], María Atienza-Martínez[3, a], Karina Hablich[4], Fernando Bimbela[4], Alfonso Cornejo[5], Luis M. Gandía[4]

[1] Biomass Laboratory, Biomass to Resources Group, Universidad Regional Amazónica IKIAM, Tena, Ecuador

[2] Centro de investigación Cepsa, Alcalá de Henares Av. Punto com, Madrid, Spain

[3] Grupo de Procesos Termoquímicos, Instituto Universitario de Investigación en Ingeniería de Aragón (I3A), Universidad de Zaragoza, Zaragoza, Spain

[4] Grupo de Reactores Químicos y Procesos para la Valorización de Recursos Renovables, Institute for Advanced Materials and Mathematics (InaMat[2]), Universidad Pública de Navarra (UPNA), Pamplona, Spain

[5] Grupo de Diseño, Síntesis Evaluación y Optimización de Nuevas Sustancias de Interés, Institute for Advanced Materials and Mathematics (InaMat[2]), Universidad Pública de Navarra (UPNA), Pamplona, Spain

(*) corresponding author: Dr. Yanet Villasana / email: yanet.villasana@kiam.edu.ec / ytvillas@gmail.com

Keywords: catalytic pyrolysis, char, residual biomass, bio-oil, cocoa.

Supporting Information

This document content the following information:

1. Experimental Section

1.1 Catalyst characterization details

1.1.1 ICP-OES

The elemental analysis of the catalysts was done by means of optical emission spectrometry with inductively coupled plasma (ICP-OES). The analysis was performed by the Servicio General de Apoyo a la Investigación (SAI) at the Universidad de Zaragoza (Spain) using a Thermo Elemental IRIS INTREPID RADIAL, equipped with a Timberline IIS automatic. The samples were dissolved prior to their analysis by microwave assisted acid digestion.

1.1.2 ICP-OES

Temperature-programmed reduction (TPR) and CO chemisorption analyses were carried out using a Micromeritics AUTOCHEM II 2920 equipped with a TCD detector. The TPR experiments were carried out selecting a final temperature of 900 ºC, which was attained following a 5 ºC/min ramp, as indicated in a previous work [1]. As for the CO chemisorption analysis, they were carried out at 35 ºC using diluted CO flow (10 vol. % CO in He). Prior to the chemisorption, the catalysts were reduced under H_2 flow for 3 h at 500 ºC. Further details on the CO chemisorption analyses can be found elsewhere [2].

It is widely accepted that CO as a well-probe molecule for determination of active surface area, and some author has assumed for simplicity that CO adsorb only on Ni surface in NiMo catalyst [3]. However, other studies have noted that Mo^{X+} species and alumina support can contribute to CO uptake [4,5]. Different modes of adsorption have been proposed for CO adsorption over metallic surface, e.g. linear, bridged and carbonyl, causing different CO/Metal stoichiometry that makes interpretation of this data not trivial. Nevertheless, in this work the results presented in the Table 2 were recorded by using CO/Metal ratio as a linear chemisorption (stoichiometry factor equal to 1, using the Equation 1) [3].

$$S_{AC}(m^2 g^{-1}) = n \cdot \frac{V_A}{V_{mol}} \cdot N_A \cdot Cs \cdot \frac{1}{m} \qquad (Eq.1)$$

where n is the stoichiometry factor according the type of adsorption, V_A is the volume of CO chemisorbed, V_{mol} is the molar volume of CO at STP conditions (cm^3/mol), N_A is the Avogadro's number, Cs is atomic cross-sectional area, which is 0.0649 nm^2/atom and 0.0730 nm^2/atom for nickel and molybdenum respectively.

1.1.3 N_2 adsorption

N_2 adsorption-desorption isotherms were measured at 77 K using a static volumetric method in a Micromeritics Gemini V automated analyzer. Prior to the analyses, the samples were conditioned by degassing at 200 ºC for 2 h under N_2 flow. Surface areas were determined by means of the Brunauer-Emmet-Teller equation (BET method) [6], whilst the total volume of pores could be estimated from the amount of N_2 adsorbed at a relative pressure of 0.99. As concerns pore size distributions, these were calculated from the isotherms by applying the Barrett-Joyner-Halenda equation [7].

1.1.4 X-ray diffraction (XRD)

X-ray diffraction analysis of the $MoNi/Al_2O_3$ catalyst was done in the Servicio de Difracción de Rayos X y Análisis por Fluorescencia of the Servicio General de Apoyo a la Investigación (SAI) at the Universidad de Zaragoza (Spain). Data were taken by means of a D-Max Rigaku Ru300 diffractometer, equipped with a Cu rotating anode. The diffractometer is operated at 40 kV and 80 mA using a graphite monochromator to select the CuKα radiation. The measurements were conducted using the following conditions: 2Θ = 5º - 95º, step = 0.03, t = 1 s/step. The JCPDS-International Centre for Diffraction Data- 2000 database was used for identifying the crystalline phases.

1.1.5 Temperature-programmed oxidation coupled to mass spectrometry (TPO-MS).

Temperature-programmed oxidation coupled to mass spectrometry (TPO-MS) runs of selected spent samples were carried out at the Instituto de Carboquímica (ICB-CSIC, Zaragoza, Spain). The analyses were conducted in a Micromeritics AUTOCHEM II 2920 equipped with a thermal conductivity (TCD) detector and coupled to an OMNISTAR mass spectrometer equipped with a Channeltron detector. The TPO experiments were developed following a 5 ºC/min temperature ramp using 50 N cm^3/min of diluted oxygen (8% O_2 in Ar) until a final temperature of 900 ºC was reached. The amount of carbon deposited on the spent samples could be determined by quantitative analysis, following the characteristic m/z signal of CO_2 emitted in the oxidation of the deposits during the TPO experiments.

1.2 Details of the Gas Chromatograph (GC)-Flame Ionization Detector (FID) analysis

The chemical composition of the liquid phases was semi-quantitatively analyzed using an Agilent 7890A Gas Chromatograph (GC)-Flame Ionization Detector (FID) system coupled with an Agilent 5975C Inert Mass Spectrometry Detector (MS) and equipped with capillary columns of different polarity. The compounds were identified by the National Institute of Standards and Technology (NIST) library. A mid-polar column Agilent DB-17ms (virtually equivalent to (50%-phenyl)-methylpolysiloxane) was used to analyze the OP. The column was held at 50 °C for 5 min and the temperature program followed by heating to 80, 200, 236, 250 and 320 °C at 1.5, 1.5, 3, 1.5 and 5 °C min^{-1}, respectively. During the program, heating was held at 80 °C (15 min), 250 °C (5 min), and 320 °C (20 min). A high-polar column Agilent HP-FFAP (nitroterephthalic acid modified polyethylene glycol) was used to analyze the AP. The column was initially held at 40 °C for 5 min and then heated to 50, 125, and 230 °C at 1, 10 and 2 °C min^{-1}, respectively. Heating was held at 230 °C for 5 min.

1.3 Details on NMR sample preparation and analysis

NMR samples for the OP were prepared at 1 % w/w in DMSO-d_6 and referenced using residual signal from DMSO-d_6 at 2.50 ppm and 39.51 ppm for ^1H and ^{13}C measurements. Samples for the AP were prepared adding 100 µL D_2O to 400 µL of sample and referenced to 4.70 ppm in ^1H measurements using the residual signal of H_2O. ^1H experiments were run using the *zg30* pulse program at 16 scans. ^{13}C measurements were carried using C13APT preinstalled experiment with a *jmod* pulse program at 4000 scans. Two dimensional ^1H- ^{13}C correlation was done using Heteronuclear Single-Quantum Correlation-Total Correlation Spectroscopy (HSQC-TOCSY)

correlations that run *hsqcdietgpsisp.2* pulse program in an echo-antiecho acquisition mode with D1 2.0 s. Diffusion Ordered Spectroscopy, DOSY, was run using *stebpgp1s*. Diffusion delay (d20) was optimized at each experiment keeping gradient pulse length (p30) constant at 1000 ms, resulting in 160-170 ms depending on the sample, to achieve 5 % residual DMSO signal at 95 % gradient strength using 1D DOSY experiment *stebpgp1s1d.* Each pseudo-2D experiment consisted of a series of 16 spectra and spectra were processed using the preinstalled Dynamic Center on Topspin 3.2 Bruker software.

2. Results and Discussion

2.1 Additional details of catalysts properties

XRD patterns:

The face centered cubic alumina phase signals found correspond to γ-Al_2O_3 with reflection maximums at 2Θ = 37,64°; 45,83° and 66,82°, associated to (3 1 1), (4 0 0) and (4 4 0) planes, respectively. Orthorhombic MoO_3 peaks were found at 2Θ = 33.76° (1 1 1); 39.00° (0 6 0); 49.28° (0 0 2), while cubic NiO crystalline phase revealed peaks at 37.28° (1 1 1); 43.31° (2 0 0) and 62.96° (2 2 0). $NiMoO_4$ monoclinic primitive were subtlety found at 2Θ values of 37,14°; 39,58° and 55,12° corresponding to (0 0 2), (2 2 0) and (2 2 1) planes, respectively.

N_2 physisorption

Regarding adsorption-desorption isotherms of fresh catalyst, Figure 1S showed a profile similar to IV type according to Brunauer [8], with a De Boer hysteresis loop type E [9] or H_2 according to IUPAC [10]. This type of isotherm is attributed to the species with mesoporosity, and the hysteresis of this type is the characteristic of the spheroidal cavities, voids between compactly packed spherical particles or with pores in the shape of an ink bottle. In addition, BJH pore size distributions are similar in all catalysts confirming the mesoporous nature of the material (Figure 2S).

2.2 Detailed discussion on Thermogravimetric analysis of Amazonian cocoa pod husks

The thermogravimetric analysis (TGA) curve of Amazonian cocoa pod husks and its first derivative (DTG) are shown in Figure 3S. Drying was observed up to 120 ºC. The weight loss in this first stage corresponded well with the moisture content in the cocoa pod husks (7.4 wt. %). Decomposition started at around 125 ºC and the DTG curve showed two maximum weight loss rate peaks at 270 and 310 ºC, respectively, related to the thermal decomposition of hemicellulose and cellulose [11]. A slower weight loss rate was observed from 310 ºC that is associated to decomposition of both cellulose and lignin. The final residue at 500 ºC accounted for around 38.9 wt. % of the initial cocoa pod husks mass. The results from the thermogravimetric study agree with previous data from the literature [12,13], in which similar weight loss regimes were observed. These results confirm that this waste is suitable for pyrolysis processes due to its relatively easy thermal decomposition.

2.3 Detailed discussion on NMR results:

^{13}C NMR signals at 177.7 ppm and 21.4 ppm confirmed that acetic acid was the major organic compound in the AP. Signals in the ranges of 190-210 ppm, 160-180 ppm and 100-140 ppm confirmed the presence of aldehydes/ketones, carboxylic acids, and aromatic compounds in the sample, respectively. Signals in the range of 45-70 ppm confirmed the presence of alkyl-oxy

moieties whereas those in the range of 15-45 ppm can be assigned to aliphatic compounds [2]. Noteworthy, carbohydrate signals in the range of 80-105 ppm were not found, pointing to total degradation of these compounds. HSQC-TOCSY provided additional insight about the composition of the OP, showing very similar cross-peaks in all cases, being the most relevant the cross-peak at 3.74-55.4 ppm, which evidenced the presence of methoxy groups in the sample [14–16]. HSQC-TOCSY crossed peaks (Table 1S) in the aromatic region confirmed the presence of phenolic, guaiacyl and vanillin units in the samples which agrees with the O-containing aromatic fraction (Figure 4 of the manuscript). Thus, crossed-peaks at 6.57-115.2 ppm, 6.74-115.0 ppm and 6.74-118.5 ppm evidenced the presence of guaiacyl units, whereas the presence of phenol units in the sample was evidenced by the cross-peaks at 6.74-118.5 ppm and 6.74-129.0 ppm and 7.16-129.0 ppm [16]. The presence of vanillin was less evident given that only 6.94-114.7 ppm cross-peak was found, together with a low intensity signal at 6.97-126.1 ppm (Figure 4S). Although signals corresponding to carbonyl groups could not be found in the ^{13}C spectra from the OP, HSQC-TOCSY signals corresponding to their C_α were detected at 2.16-20.2 ppm and 2.10-15.8 ppm suggesting the presence of aliphatic ketones. DOSY-NMR is a pseudo 2D experiment that provides the diffusion coefficient, D, of the sample at a given temperature. As stated in the Stokes-Einstein equation [17], D is directly related to the hydrodynamic radius of the diffusate. Therefore, D measurements provide similar information than Size Exclusion Chromatography and can be envisaged as a NMR-chromatographical tool[18]. DOSY-NMR measurements on the OP showed two significant diffusion traces could be found in all the analyzed samples, either in pyrolysis or pyrolysis followed by downstream catalytic treatment of the hot vapors at log D -9.406 and -9.468 (Figure 6S). As it can be seen in Table 2S and Table 3S of SI, these values are like those measured for guaiacol and vanillin, respectively, and much lower than that measured for an analytical standard of polystyrene with M_w 370 Da. Therefore, these log D values suggest that the OP contained mainly monomeric units with guaiacyl and vanillin moieties, as it was pointed by HSQC-TOCSY. This was confirmed by the extension of the diffusion traces in the aromatic region, the methoxy group region (*ca.* 3.75-4.00 ppm) and the ketones H_α region (2.0-2.2 ppm). Indeed, GC-MS analysis stated the presence of individual ketones that may present similar hydrodynamic radii than guaiacyl and vanillin moieties. The extension of the traces to higher fields (d< 2.0 ppm) suggested the presence of alkyl side chains in the aromatic compounds. Additionally, in the case of the MoNi/γ-Al_2O_3 catalyzed reaction, a slight trace was observed at logD -9.345, that suggested the presence of lower hydrodynamic radii, probably phenol or *o*-cresol, according to the logD values shown in Table 3S.

2.4 Additional Figures and Tables

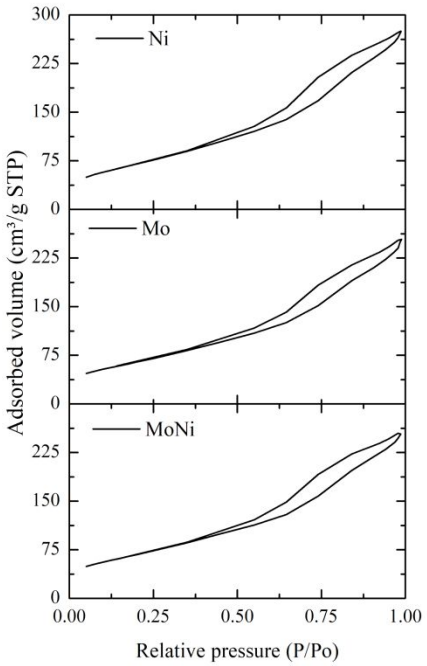

Figure 1S. Adsorption-desorption isotherms of fresh catalysts (pre-reduced and passivated).

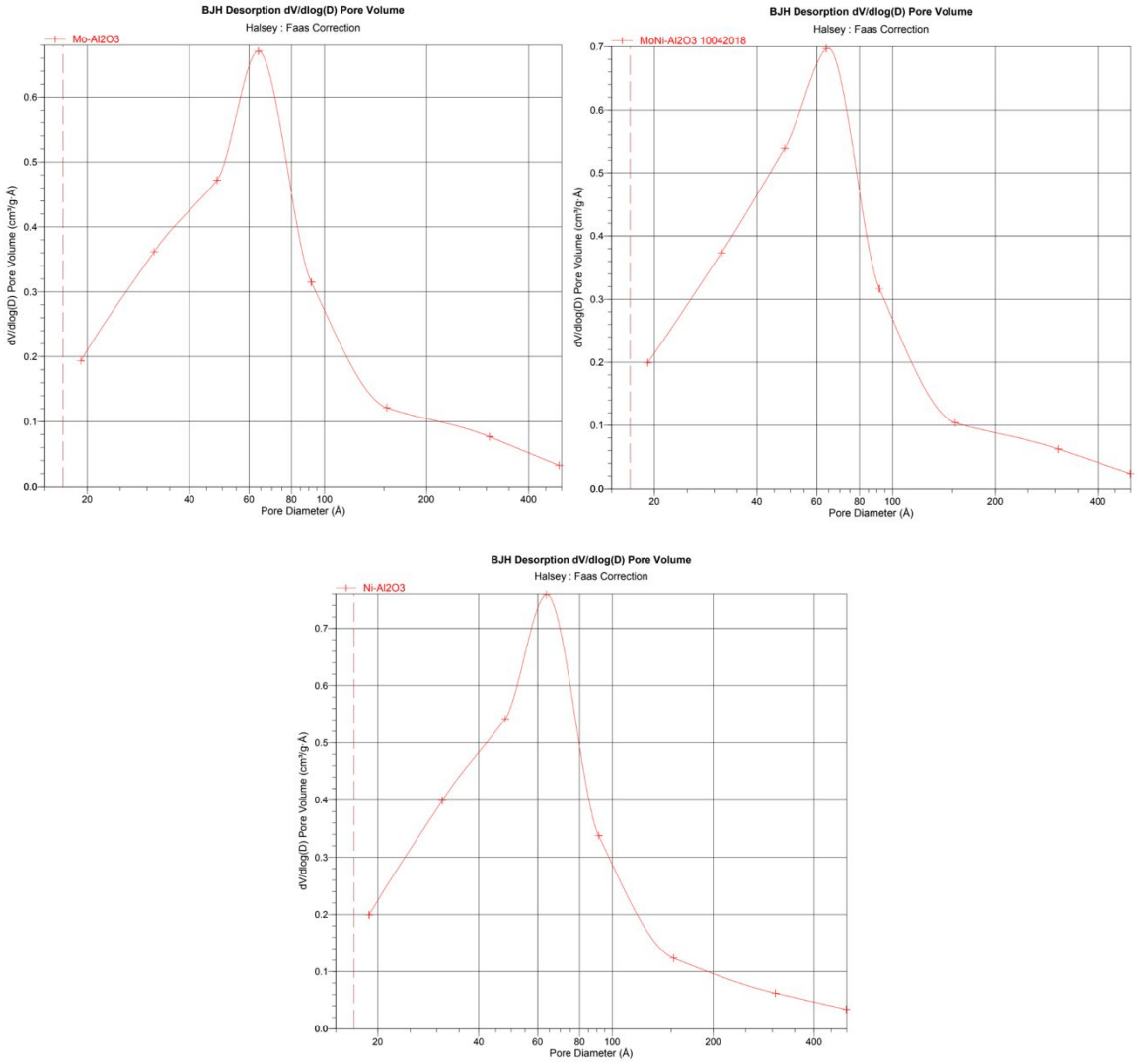

Figure 2S. BJH pore size distribution of catalysts original report from the Micromeritics Instrument.

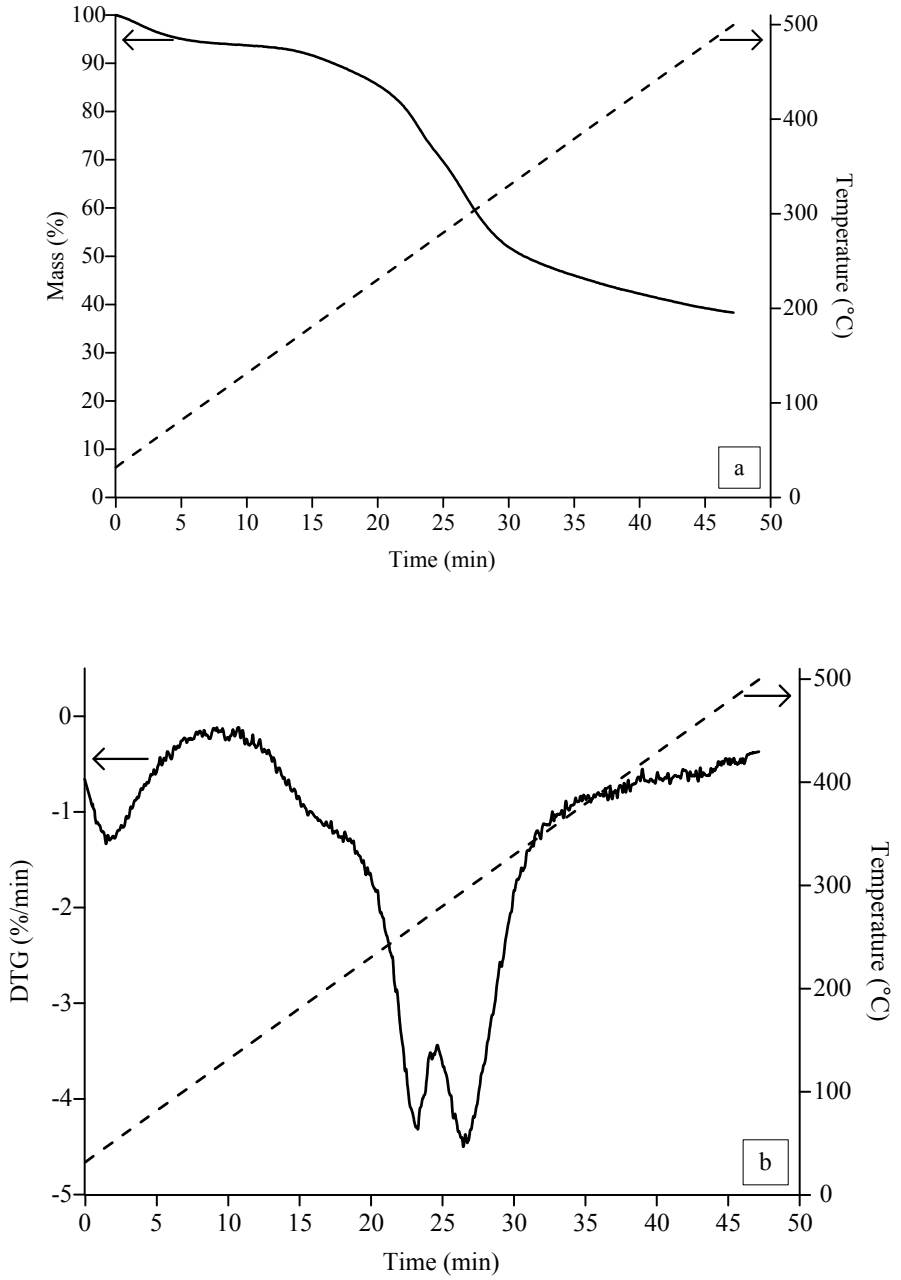

Figure 3S. a) TG and b) DTG profiles for Amazonian cocoa pod husks pyrolysis.

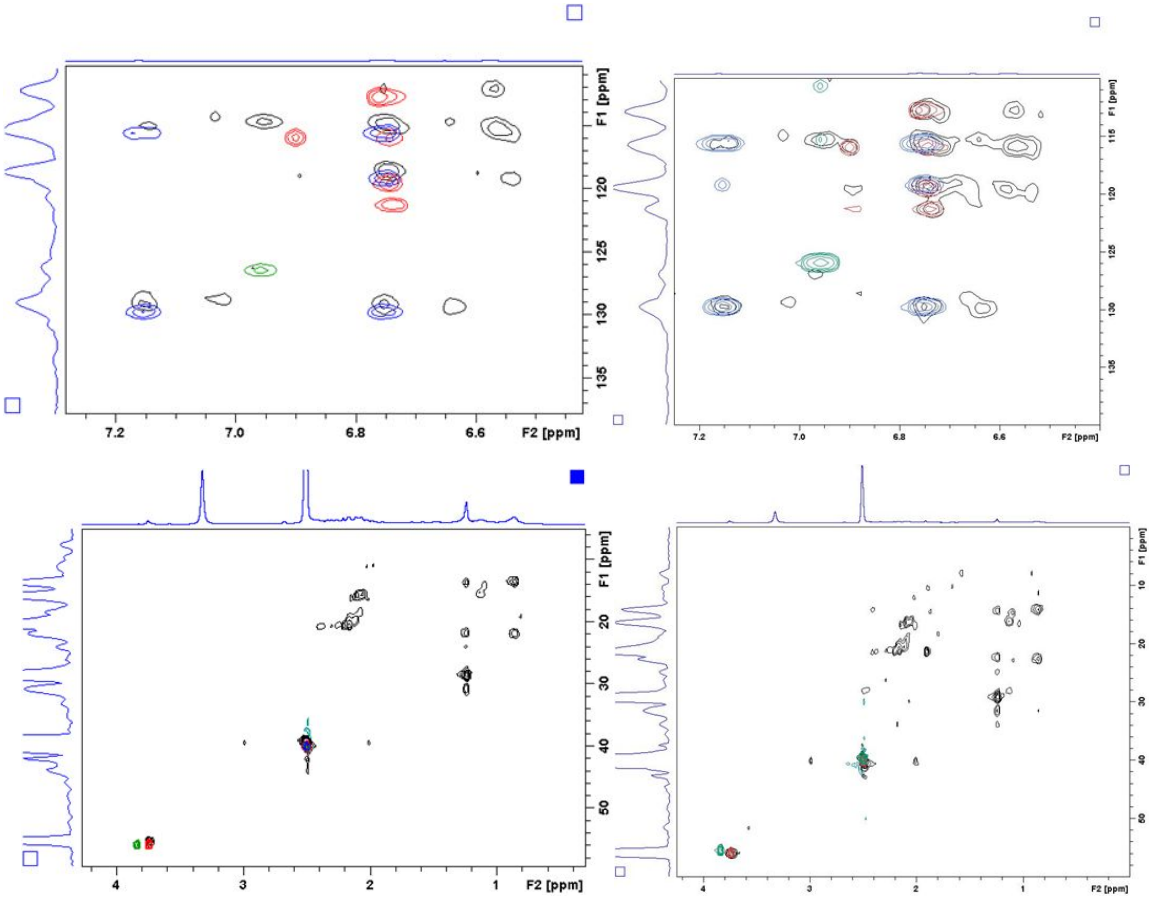

Figure 4S. HSQC-TOCSY spectra corresponding to non-catalyzed reaction (black, left), and MoNi/Al_2O_3 RP (black, right) phenol (blue), guaiacol (red) and vanillin (green).

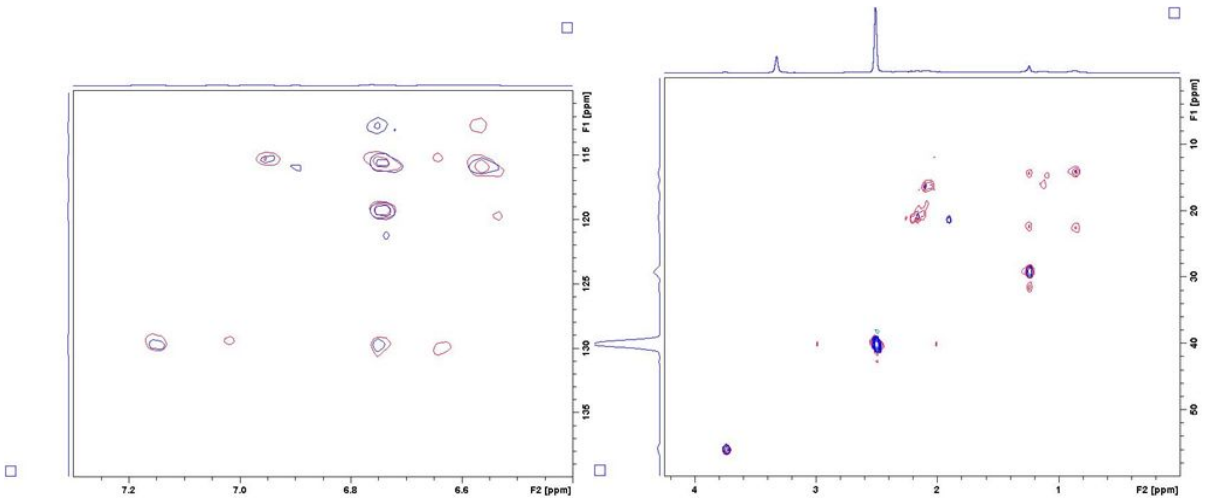

Figure 5S. HSQC-TOCSY spectra corresponding to for non-catalyzed reaction (red) and MoNi/Al_2O_3 RP (blue).

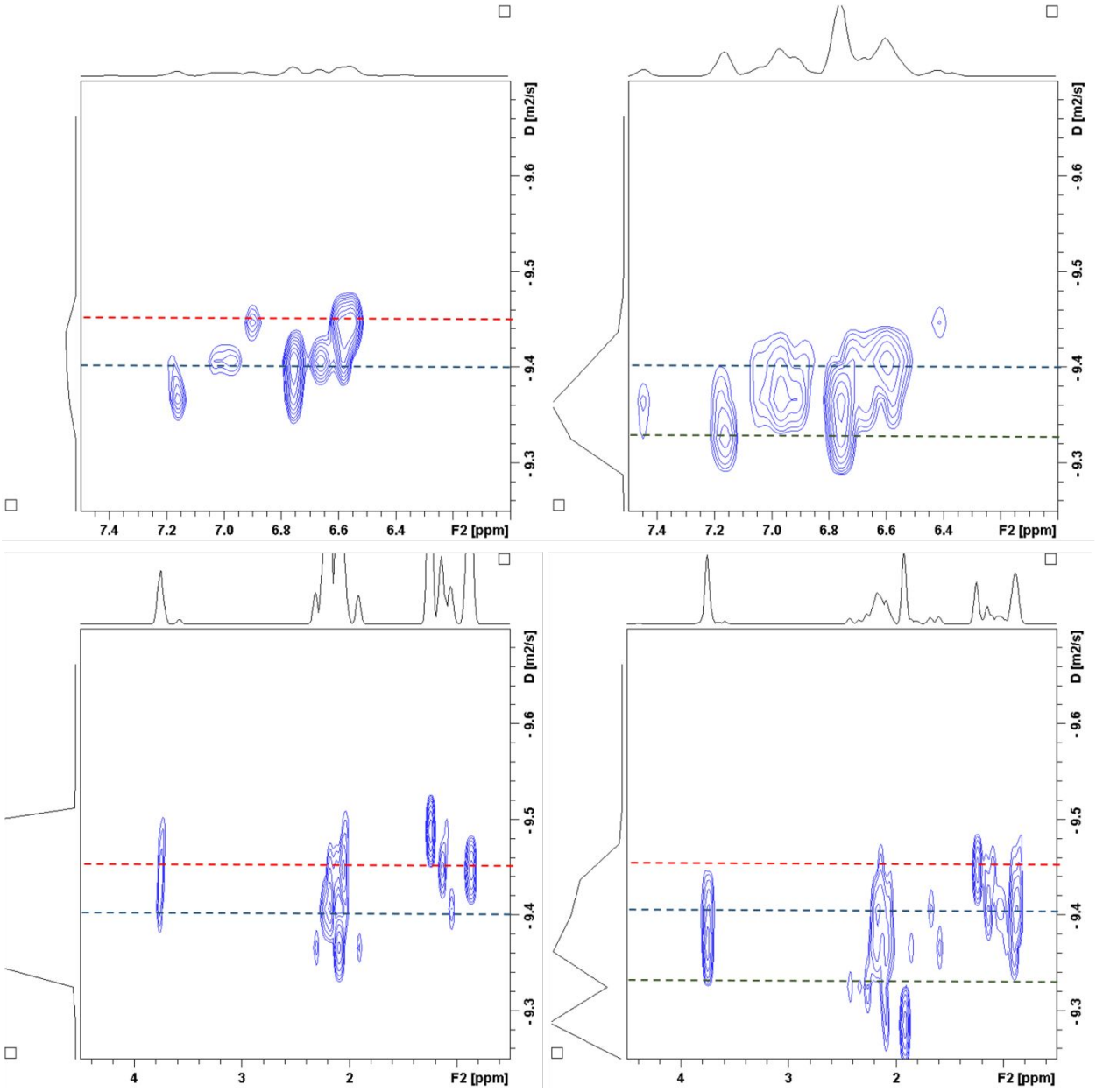

Figure 6S. DOSY spectra for non-catalyzed reaction (left) and MoNi/γ-Al_2O_3 (right) in the aromatic region (top) and in the methoxy and aliphatic regions (bottom). Red dotted line corresponds to logD -9.46 black dotted line to logD -9.40, and green dotted line to logD -9.34

Table 1S. Relevant cross-peaks in the HSQC-TOCSY.

^{1}H ppm	**^{13}C ppm**	**Assignment**
6.36	112.63	G2, G5 and G6
6.57	112.16	C5-H5’
6.57	115.21	C6-H6’ in guaiacyl units
6.63	129.28	Cinnamyl alcohol
6.74	114.97	C2-H2 in guaiacyl units
6.74	118.49	C2-H2 in guaiacyl units, phenols
6.75	129.04	Phenol units
6.94	114.74	C2-H2 in guaiacyl units, vanillin units
6.97	126.23	Vanillin unit, H6
7.16	129.04	2,6-hydroxymethyl phenol
7.16	114.98	Phenol
3.75	55.4	C-H in methoxyls

Table 2S. Log D for phenolic and hydrocarbon analytical standards.

Compound	**-Log D (m2/s)**
Phenol	9.321
Guaiacol	9.406
Vanillin	9.465
2,6-dimethoxyphenol	9.431
PS 370 Da	9.588
DMSO	9.157

Table 3S. Log D for different traces the OP.

Sample	Trace	-Log D (m2/s)
OP from non-Catalytic pyrolysis	Aromatic 1	9.405
	Aromatic 2	9.466
	Methoxy 1	9.408
	Methoxy 2	9.467
	Aliphatic 1	9.407
	Aliphatic 2	9.468
	Aliphatic 3	9.531
	DMSO	9.154
OP from MoNi/γ-Al_2O_3 *ex-situ* pyrolysis	Aromatic 1	9.405
	Aromatic 2	9.466
	Methoxy 1	9.405
	Methoxy 2	9.467
	Aliphatic 1	9.407
	Aliphatic 2	9.467
	Aromatic 1	9.345
	Methoxy 1	9.345
	DMSO	9.157

References

(1) Moral, A.; Reyero, I.; Alfaro, C.; Bimbela, F.; Gandía, L. M. Syngas Production by Means of Biogas Catalytic Partial Oxidation and Dry Reforming Using Rh-Based Catalysts. *Catal. Today* **2016**, No. March, 0–1. https://doi.org/10.1016/j.cattod.2017.03.049.

(2) Carrier, M.; Windt, M.; Ziegler, B.; Appelt, J.; Saake, B.; Meier, D.; Bridgwater, A. Quantitative Insights into the Fast Pyrolysis of Extracted Cellulose, Hemicelluloses, and Lignin. *ChemSusChem* **2017**, *10* (16), 3212–3224. https://doi.org/10.1002/cssc.201700984.

(3) Yin, W.; Venderbosch, R. H.; Alekseeva, M. V; Figueirêdo, M. B.; Heeres, H.; Khromova, S. A.; Yakovlev, V. A.; Cannilla, C.; Bonura, G.; Frusteri, F.; Heeres, H. J. Hydrotreatment of the Carbohydrate-Rich Fraction of Pyrolysis Liquids Using Bimetallic Ni Based Catalyst: Catalyst Activity and Product Property Relations. *Fuel Process. Technol.* **2018**, *169*, 258–268. https://doi.org/https://doi.org/10.1016/j.fuproc.2017.10.006.

(4) Bartholomew, C. H.; Pannell, R. B. The Stoichiometry of Hydrogen and Carbon Monoxide Chemisorption on Alumina- and Silica-Supported Nickel. *J. Catal.* **1980**, *65* (2), 390–401. https://doi.org/https://doi.org/10.1016/0021-9517(80)90316-4.

(5) Williams, C. C.; Ekerdt, J. G. Infrared Spectroscopic Characterization of Molybdenum Carbonyl Species Formed by Ultraviolet Photoreduction of Silica-Supported Molybdenum(VI) in Carbon Monoxide. *J. Phys. Chem.* **1993**, *97* (26), 6843–6852. https://doi.org/10.1021/j100128a017.

(6) Brunauer, S.; Emmett, P. H.; Teller, E. Adsorption of Gases in Multimolecular Layers. *J. Am. Chem. Soc.* **1938**, *60* (2), 309–319. https://doi.org/10.1021/ja01269a023.

(7) Rouquerol, F.; Rouquerol, J.; Sing, K. S. W. The Experimental Approach. In *Handbook of Porous Solids*; 2002; pp 236–275. https://doi.org/https://doi.org/10.1002/9783527618286.ch7a.

(8) Mikhail, R. S.; Brunauer, S. Surface Area Measurements by Nitrogen and Argon Adsorption. *J. Colloid Interface Sci.* **1975**, *52* (3), 572–577.

(9) De Boer, J. H. The Shapes of Capillaries. In *The Structure and Properties of Porous Materials*; Everett, D. H., Stone, F. S., Eds.; Butterworths: London, 1958; p 68.

(10) Leofanti, G.; Padovan, M.; Tozzola, G.; Venturelli, B. Surface Area and Pore Texture of Catalysts. *Catal. Today* **1998**, *41* (1), 207–219. https://doi.org/https://doi.org/10.1016/S0920-5861(98)00050-9.

(11) Mansur, D.; Tago, T.; Abimanyu, H. Conversion of Cacao Pod Husks by Pyrolysis and Catalytic Reaction to Produce Useful Chemicals. **2014**, No. July. https://doi.org/10.1016/j.biombioe.2014.03.065.

(12) Titiloye, J. O.; Abu Bakar, M. S.; Odetoye, T. E. Thermochemical Characterisation of Agricultural Wastes from West Africa. *Ind. Crops Prod.* **2013**, *47*, 199–203. https://doi.org/10.1016/j.indcrop.2013.03.011.

(13) Tsai, C.-H.; Tsai, W.-T.; Liu, S.-C.; Lin, Y.-Q. Thermochemical Characterization of Biochar from Cocoa Pod Husk Prepared at Low Pyrolysis Temperature. *Biomass Convers. Biorefinery* **2018**, *8* (2), 237–243. https://doi.org/10.1007/s13399-017-0259-5.

(14) Kuznetsov, B. N.; Chesnokov, N. V.; Sudakova, I. G.; Garyntseva, N. V.; Kuznetsova, S. A.; Malyar, Y. N.; Yakovlev, V. A.; Djakovitch, L. Green Catalytic Processing of Native and Organosolv Lignins. *Catal. Today* **2018**, *309* (December 2017), 18–30. https://doi.org/10.1016/j.cattod.2017.11.036.

(15) Rencoret, J.; Marques, G.; Gutiérrez, A.; Nieto, L.; Santos, J. I.; Jiménez-Barbero, J.; Martínez, Á. T.; Del Río, J. C. HSQC-NMR Analysis of Lignin in Woody (Eucalyptus Globulus and Picea Abies) and Non-Woody (Agave Sisalana) Ball-Milled Plant Materials at the Gel State. *Holzforschung* **2009**, *63* (6), 691–698. https://doi.org/10.1515/HF.2009.070.

(16) Wen, J. L.; Sun, S. L.; Yuan, T. Q.; Xu, F.; Sun, R. C. Structural Elucidation of Lignin Polymers of Eucalyptus Chips during Organosolv Pretreatment and Extended Delignification. *J. Agric. Food Chem.* **2013**, *61* (46), 11067–11075. https://doi.org/10.1021/jf403717q.

(17) Li, D.; Kagan, G.; Hopson, R.; Williard, P. G. Formula Weight Prediction by Internal Reference

Diffusion-Ordered NMR Spectroscopy (DOSY). *J. Am. Chem. Soc.* **2009**, *131* (15), 5627–5634. https://doi.org/10.1021/ja810154u.

(18) Ge, W.; Zhang, J. H.; Pedersen, C. M.; Zhao, T.; Yue, F.; Chen, C.; Wang, P.; Wang, Y.; Qiao, Y. DOSY NMR: A Versatile Analytical Chromatographic Tool for Lignocellulosic Biomass Conversion. *ACS Sustain. Chem. Eng.* **2016**, *4* (3), 1193–1200. https://doi.org/10.1021/acssuschemeng.5b01259.